ANNUAL REVIEWS

Annual Review of Analytical Chemistry

Lipid Diversity in Cells and Tissue Using Imaging SIMS

Sanna Sämfors[1,2] and John S. Fletcher[1]

[1]Department of Chemistry and Molecular Biology, University of Gothenburg, 41296 Gothenburg, Sweden; email: john.fletcher@chem.gu.se

[2]Department of Chemistry and Chemical Engineering, Chalmers University of Technology, Gothenburg, Sweden

Annu. Rev. Anal. Chem. 2020. 13:249–71

First published as a Review in Advance on March 25, 2020

The *Annual Review of Analytical Chemistry* is online at anchem.annualreviews.org

https://doi.org/10.1146/annurev-anchem-091619-103512

Keywords

secondary ion mass spectrometry, SIMS, imaging, lipids, cells, tissue

Abstract

Lipids are an important class of biomolecules with many roles within cells and tissue. As targets for study, they present several challenges. They are difficult to label, as many labels lack the specificity to the many different lipid species or the labels maybe larger than the lipids themselves, thus severely perturbing the natural chemical environment. Mass spectrometry provides exceptional specificity and is often used to examine lipid extracts from different samples. However, spatial information is lost during extraction. Of the different imaging mass spectrometry methods available, secondary ion mass spectrometry (SIMS) is unique in its ability to analyze very small features, with probe sizes <50 nm available. It also offers high surface sensitivity and 3D imaging capability on a subcellular scale. This article reviews the current capabilities and some remaining challenges associated with imaging the diverse lipids present in cell and tissue samples. We show how the technique has moved beyond show-and-tell, proof-of-principle analysis and is now being used to address real biological challenges. These include imaging the microenvironment of cancer tumors, probing the pathophysiology of traumatic brain injury, or tracking the lipid composition through bacterial membranes.

INTRODUCTION

Lipids are biologically important molecules involved in many biochemical processes within cells. They have various functions as structural components in cell membranes or as signaling molecules, and they are used for energy storage (1). Lipids are defined as organic molecules that occur naturally and are insoluble in water but soluble in nonpolar organic solvents. There is great variety in the structure of lipids, and they have been divided into different classes based on their structure (2, 3). Most lipids found in biological systems are amphiphilic, consisting of both a hydrophobic and hydrophilic part. Therefore, in aqueous environments, they can form structures such as membranes, which makes them useful building blocks for cells. The cell membrane consists of proteins and lipids, and the great structural variety of both types of molecules provides a means of tuning the membrane properties depending on the required function (4, 5). The lipids and proteins interact in the cell membrane, and it has been shown that lipids can alter the protein function based on the difference in interaction depending on lipid type (6). All organelles in the cells are surrounded by lipid membranes, and different lipid compositions and protein compositions provide different functions in the cell (7). Changes in membrane composition have been shown to occur in response to different external stimuli. For example, lipid composition alteration, in response to temperature change, that affects membrane fluidity has been observed in a variety of cells and organisms, and changes in lipid composition of cells and tissues have been connected to various disease processes (8, 9). This is why in recent years lipidomics studies have become important when the entire lipid population of a cell or organ is studied (10).

Different methods for quantitative analysis have been developed, such as thin-layer chromatography (11), high-performance liquid chromatography (12), and enzyme-based fluorometric methods (13), but these methods do not provide any spatial information about the lipids in cells or tissues. Some imaging methods have been employed to study the lipid composition in specific parts of the studied cells or tissues, such as fluorescence imaging (14, 15), but this requires labeling with fluorescent tags that are usually quite large compared to lipid molecules that could alter the natural behavior and structure of the molecule(s) being studied. Recently, the use of different mass spectrometry methods for lipid analysis has become of interest. In particular, imaging mass spectrometry techniques, such as time-of-flight secondary ion mass spectrometry (ToF-SIMS), have been shown to be useful for in situ lipid analysis of various biological samples. This is because lipids provide an excellent analytical target for ToF-SIMS imaging owing to the ionization and sputtering properties of many lipid species.

SIMS for Lipid Imaging

SIMS utilizes an energetic (typically tens of kilo electron volts) primary ion that, upon impact with a sample surface usually under high vacuum conditions, leads to the ejection of secondary species via a process called sputtering. A small proportion of these secondary species are charged, and these secondary ions can be extracted and fed into a mass spectrometer. Compared to other desorption ionization mass spectrometry approaches, for example, matrix-assisted laser desorption mass spectrometry (MALDI-MS) and desorption electrospray ionization mass spectrometry (DESI-MS), SIMS is unique in that the depth of origin of the analyte ions can be extremely shallow, providing very high surface sensitivity. Further, some of the ion beams used in SIMS can be focused to produce spot sizes of <50 nm on the sample surface. Historically, SIMS has been employed in two modes: static mode and dynamic mode. Most lipid analysis with SIMS has been performed in the static mode using various types of ToF mass spectrometers because detection of intact molecules was not possible in the dynamic mode. However, as is discussed later, the traditional distinctions between the two modes have become more blurred (see sidebar titled Static and Dynamic SIMS).

STATIC AND DYNAMIC SIMS

Static SIMS infers that the spectrum represents the pristine surface chemistry by meeting the condition that <1% of the surface is affected by using a low primary ion dose density. The accumulation of subsurface chemical damage meant that, for many years, all molecular analysis was performed in this mode. In dynamic SIMS, secondary ion signal intensities are monitored as the sample is eroded by the ion beam. Historically, this was limited to the detection of atomic or very small fragment ions and is used widely for inorganic analysis especially in the semiconductor industry.

Lipid analysis with SIMS has been performed on a myriad of samples where cells or cell populations have been investigated in studies. This includes imaging analysis to investigate the natural lipid composition where large cells such as snail neurons and frog eggs presented good opportunities for imaging lipid signals from single cells in 2D and 3D (16, 17). Changes in lipid composition have also been monitored in developing embryos, and differences in lipid composition of cancer cell lines have been studied (18, 19). SIMS studies have also been used to show how changes in lipid composition can be related to changes in cell function, such as exocytosis events in phaeochromocytoma (PC)12 cells after lipid changes caused by zinc exposure (20). Lipid analysis on tissue has also been performed by many laboratories on samples ranging from clinical biopsy samples and mammalian animal models to fly, fish, and worm samples, to list but a few (21–27).

This review describes the developments in SIMS that are helping to increase the diversity of the lipidome that can be probed in situ and potentially imaged in 2D and sometimes 3D at high spatial resolution. These developments include changes in the nature of the primary ion beam used in the analysis, the type of mass analyzer used to collect the data, and approaches to sample preparation.

TOF-SIMS FOR CELLULAR LIPID IMAGING

The most common primary ion beams used in ToF-SIMS instruments are liquid metal ion sources, including those producing small clusters such as Au_3^+ or Bi_3^+ (28, 29). These high brightness sources are extremely practical and versatile and can be focused to produce spot sizes <50 nm on the sample surface. However, at such spatial resolution the ability to characterize lipid species is greatly diminished. There are two main reasons for this. The first is a simple issue of the number of target analyte molecules in the pixel area; as the area is decreased, the amount of analyte decreases and challenges the sensitivity of the instrument. This is true for all imaging MS modalities and also depends on the ionization efficiency of the analyte molecules in the pixel; ejected neutral species will not be detected by the mass spectrometer. The second factor, which compounds the reduced analyte problem, is that the aforementioned ion beams are inefficient at generating intact lipid signals. These ion beams generally produce secondary ions from small molecules (up to several hundred daltons) or fragments of larger molecules that are formed during the ejection process.

The best chance for detecting characteristic lipid signals at this spatial resolution with these beams comes from the phosphatidylcholine (PC) head group that produces a very intense signal at m/z 184. As a consequence, this species has become one of the most imaged ion species in biological SIMS studies.

Sjövall and coworkers (30) tested the ability to image different types of lipid vesicles using a liquid metal ion beam. This image resolution study utilized the intense PC head group signal to detect liposomes formed from dipalmitoylphosphatidylcholine (DPPC) and distinguish

them from similar liposomes produced that contained 1-palmitoyl-2-oleoyl-*sn*-glycero-3-ethylphosphocholine (POEPC) and where the presence of the phosphate-bound ethyl group produced an additional peak at *m/z* 212 along with the *m/z* 184 ion. This study demonstrated the powerful imaging capabilities of the technique that could identify individual 300±100-nm-diameter lipid vesicles, with the caveat that the target compound produced a unique and very intense signal, as shown in **Figure 1*a–c,b***.

Due to the limited signal at very small pixel size, most cellular (or even subcellular) imaging with SIMS is normally performed with pixel sizes of around 1 μm. At this spatial resolution, signals can also be detected and imaged from other lipid head group ions from different classes of glycerophospholipids. The Ewing group (31, 32) exploited this capability to investigate the changes in lipid composition during the formation of fusion pores in mating *Tetrahymena*, a freshwater dwelling protozoon, using an In^+ primary ion beam. A relative change in intensity between the *m/z* 184 PC head group ion and the *m/z* 124 peak, assigned to the head group of 2-aminoethylphosphonolipid (2-AEP), was interpreted as an enrichment of lipid species at the fusion site with relatively smaller head groups. These conical 2-AEP lipid species (as opposed to the cylindrical PC lipids) facilitated the formation of highly curved structures in the membrane (**Figure 1*d–g,i***).

The limitations associated with poor molecular ion yield from atomic or small cluster primary ion beams can sometimes be worked around if suitable characteristic fragment ions could be found in the mass spectra. Many studies have focused on the use of phospholipid head group signals (such as the aforementioned PC, *m/z* 184, signal) and also fatty acid ions originating from either free fatty acids or larger lipid species that had become fragmented during the sputtering process. These diagnostic fragment ions can often be 1 or 2 orders of magnitude higher than the intact lipid ions in the SIMS spectrum. Several examples of fatty acid imaging are shown in **Figure 2**, including the imaging of zebra finch brain, human skin, and human liver tissues (33–35).

Cholesterol falls into a mass range that is usually accessible by SIMS analysis, and the relatively stable $[M+H-H_2O]^+$ ion is often reported from biological samples. However, cholesterol esters are larger and less stable, making them difficult to detect under normal analysis conditions, directly from cells or tissue, although they can be detected following silver cationization of lipid extract samples (36). Two separate approaches to distinguish cholesterol from cholesterol esters using fragment ions have been proposed, although not widely adopted. Lee et al. (37) identified characteristic peaks in reference spectra from palmitic acid (Ch-PA) and oleic acid (Ch-OA) cholesterol esters at *m/z* 237.2 and 263.2, respectively. They used these ions to image the distribution of the different species and their ratios, suggesting that the ratio may be a marker of atherosclerosis. Lehti et al. (38) suggested that the ratio between the different forms of the pseudomolecular ions of cholesterol ($[M+H-H_2O]^+$ and $[M-H]^+$) could differentiate cholesterol from cholesterol esters.

Since the early 2000s, the high-resolution (generally 1–2 μm) imaging of SIMS using small fragments was considered to be complementary with the MALDI-MS imaging being performed at the time; the relative benefits of the two methods were discussed in articles by McDonnell & Heeren (39) and Brunelle and coauthors (40). The use of MALDI matrices to enhance secondary ion signals was demonstrated (41), and metal cationization, such as silver imprinting, was shown to be particularly useful for increasing the signal for cholesterol in single cells (42).

Increasing Lipid Molecular Ion Signal Using New Ion Beams

The quest for increased secondary ion signal for intact molecular ions drove the development of new ion beams, most significantly Au_3, Bi_3, and C_{60} (43). In an assessment of the advantages of

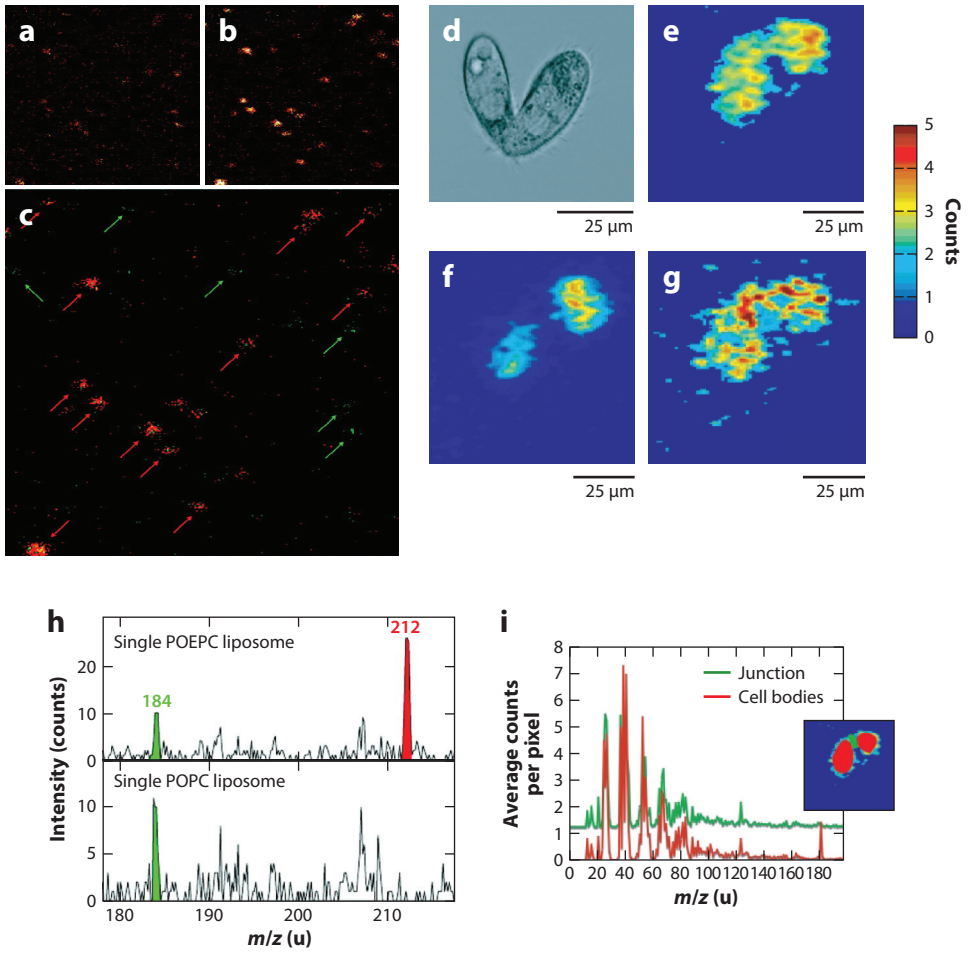

Figure 1

(*a*, *b*) Secondary ion mass spectrometry (SIMS) images of individual, freeze-dried, POPC and POEPC vesicles. Both lipids produce the fragment ion at *m/z* 184 (*a*), whereas only the POEPC lipid vesicles produce the ion at *m/z* 212 (*b*). The field of view is 50 × 50 μm^2. (*c*) Overlay of the *m/z* 184 signal from panel *a* in green and the *m/z* 212 signal panel *b* in red, with arrows highlighting the individual vesicles. (*d–g*, *i*) Imaging of a pair of mating *Tetrahymena thermophila*. (*d*) Differential interference contrast microscopy image of a mating *Tetrahymena*. (*e–g*) SIMS images showing the distribution of different ion species on the surface of the mating pair. $C_5H_9^+$ is mapped in panel *e*, the *m/z* 184 signal from phosphatidylcholine is mapped in panel *f*, and *m/z* 124, assigned to the head-group of 2-AEP lipids, is shown in panel *g* (the intensity in the 2-AEP image has been multiplied by 3). As with the vesicle imaging, mass spectra can be extracted from specific regions of interest (ROIs). Panel *i* shows the extracted mass spectrum from the cell bodies in red, whereas the green mass spectrum is from the mating junction. (*h*) Positive ion spectra from single POPC and POEPC lipid vesicles in the image. The peaks at *m/z* 184 and *m/z* 212 are clearly visible from the POEPC vesicle spectrum compared with the spectrum from the POPC vesicle that shows only the *m/z* 184 peak. Adapted with permission from Reference 30. Copyright 2010, American Chemical Society. (*i*) Inset highlights the ROIs on the SIMS image: red for the cell bodies and green for the junctions that were used to generate the corresponding mass spectra. Adapted with permission from Reference 31.

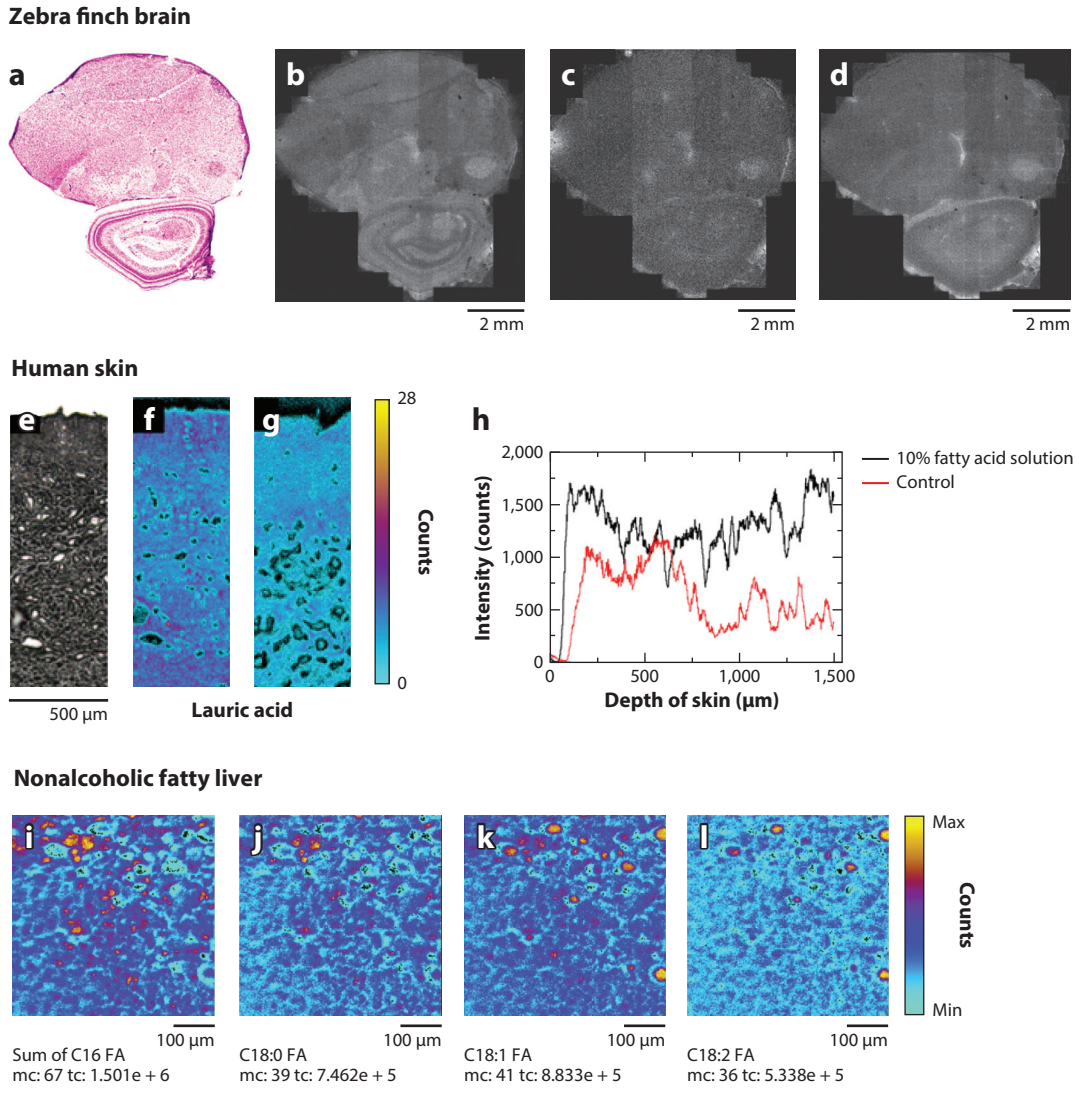

Figure 2

ToF-SIMS imaging studies of fatty acids. (*a–d*) Images of zebra finch brain slices. (*a*) Histologically stained zebra finch brain slice for determination of anatomical features. ToF-SIMS images show different fatty acid distribution of (*b*) palmitic acid C16:0 (*m/z* 255.2), (*c*) palmitoleic acid C16:1 (*m/z* 253.2), and (*d*) oleic acid C18:1 (*m/z* 281.2). Panels *a–d* adapted with permission from Reference 33. Panels *e–g* and depth profile (*h*) show fatty acid penetration into human skin. Panel *e* is an optical picture, and panels *f* and *g* are ToF-SIMS images (negative ion mode) showing the distribution of lauric acid (*m/z* 199) ion in skin (*f*) treated with 10% lauric acid solution or (*g*) control skin. Panel *h* shows average ion intensities of lauric acid as a function of depth into the skin: 10% fatty acid solution and control. Adapted with permission from Reference 34. (*i–l*) ToF-SIMS images of nonalcoholic fatty liver tissue slices, where panel *i* is the sum of C16 fatty acid carboxylate ions, panel *j* is C18:0 fatty acid (negative ion mode), panel *k* is C18:1 fatty acid, and panel *l* is C18:2 fatty acid (all detected in negative ion mode). Adapted with permission from Reference 35. Copyright 2009, American Chemical Society. Abbreviations: mc, maximum number of counts; tc, total number of counts; ToF-SIMS, time-of-flight secondary ion mass spectrometry.

these cluster and polyatomic ion beams, molecular ion signals at approximately *m/z* 1,100 from *Bacillus amyloliquefaciens* showed a 5–15× increase in signal for Au_3^+ and a 20–40× increase in signal for C_{60}^+ relative to Au^+ (44). The emergence of C_{60} as a projectile also unlocked new areas of study in molecular depth profiling and 3D molecular imaging where the signals in the SIMS analysis could be mapped both laterally and also as a function of depth into the sample as it was gradually eroded by the ion beam. On large samples such as frog eggs, it was shown that large lipid-related ions with masses in the diacylglyceride (DAG) range (typically *m/z* 450–650) could be imaged in 3D. On smaller samples such as mammalian single cells, analysis was still limited to lipid head group, fatty acid signal, or pooled signal from multiple lipids of a similar subclass (17, 45, 46). The use of C_{60}^+ to depth profile through rodent brain sections showed that during drying or vacuum exposure at room temperature, cholesterol appeared to become enriched on the surface of white matter regions of the tissue where it then masked the signals from other lipids (47–47). This confirmed earlier findings by Sjövall et al. (49).

Parallel to the introduction of C_{60}^+ primary ion beams, gas cluster ion beams (GCIBs) were developed for semiconductor processing and tested for SIMS by Matsuo and coworkers (50). The super-cooled gas clusters, formed from the expansion of pressurized gas as it enters a high vacuum chamber, are ionized by electron impact and normally size selected before being fired at the sample surface. The clusters typically comprise several thousand constituents that are most commonly atoms of a noble gas, typically Ar, or other species such as CO_2 or H_2O, as discussed below. GCIBs have found widespread use as etching guns, typically at relatively low energy for depth profile analysis of organic materials; several studies have also demonstrated their advantages as analysis beams for biological samples (51–53).

Angerer et al. (54) reported on the move to higher-energy (40-keV) gas clusters equivalent to the energy normally used for the C_{60}^+ ion beam on the same instrument. For lipid analysis, where rat brain was used as a test sample, an approximately 30–50× increase in secondary ion yield for intact lipid signals was reported compared with the C_{60}^+ analysis. A smaller relative secondary ion yield increase was noted for the smaller lipid fragment ions with an approximately 4–20× increase in signal being observed for the fatty acid species.

A recent study on the lipid changes occurring following surgically induced infarction of mouse hearts clearly demonstrates both the benefits of the GCIBs for intact lipid detection and the need for spatially resolved lipidomics. Conventional analysis of this type of sample is performed using a combination of tissue staining and liquid chromatography mass spectrometry (LC-MS) analysis of lipid extracts from the heart. Lipids are not easy to stain, and while **Figure 3** shows localization of oil red O to specific regions of the tissue, this lipid stain provides no detailed chemical specificity, only the presence of neutral lipids. In contrast, the LC-MS provides the chemical specificity of MS analysis but with no spatial information. The imaging SIMS provides the missing pieces of the puzzle. The SIMS study, using 40-keV gas clusters, showed changes in lipid species that were largely in agreement with LC-MS data. However, specific lipids showed highly localized signals in the SIMS images, such as specific phosphoinisitol lipids and acylcarnitines that localize to the border region between the damaged and healthy heart tissue (**Figure 3**). Although a general depletion of phosphoinisitol lipid signal in the infarcted region of the tissue could be explained by an increase in phospholipase activity, the accumulation of specific phosphoinisitol lipids at the border between the infarcted and noninfarcted tissue was an unexpected result.

Although GCIBs have been shown to produce significant increases in intact molecular signals from lipids, a reasonably high degree of fragmentation still occurs during the ion formation process. While not entirely desirable, such in-source fragmentation can be utilized to improve confidence in putative assignment or to elucidate some structural information if characteristic fragments and intact molecules show strong spatial correlation in the mass spectral image. In a

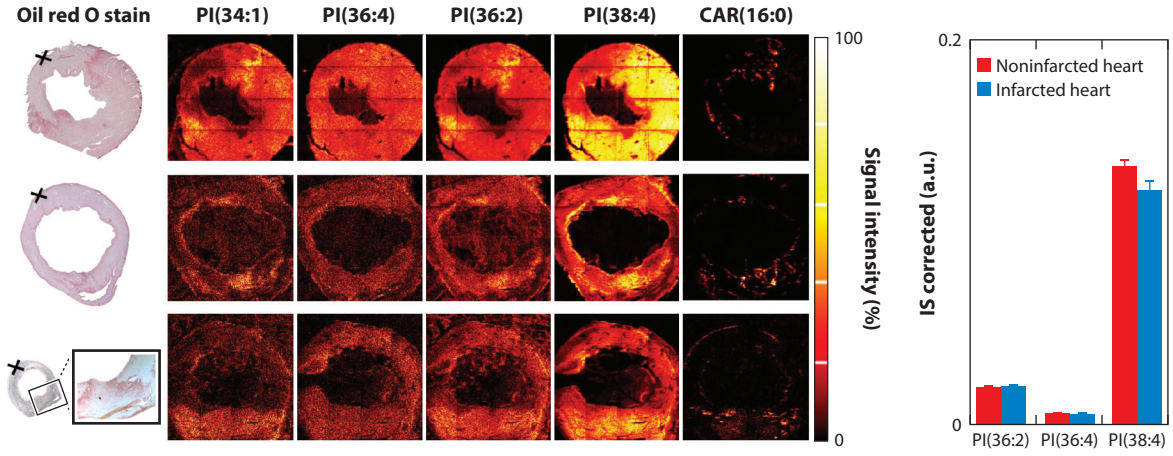

Figure 3

Infarcted mouse heart tissue analysis comparing histology images (stained with oil red O) with mass spectrometric imaging. Single ion images of $[M\text{-}H]^-$ ions of phosphatidylinositol species PI(34:1), PI(36:4), PI(36:2), and PI(38:4) (*m/z* 835, *m/z* 857, *m/z* 861, and *m/z* 885, respectively) and the $[M+H]^+$ ion of acyl-carnitine CAR(16:0) (*m/z* 400). Bar graph shows liquid chromatography mass spectrometry (LC-MS) data for the same PI species normalized to an internal standard (IS). Ion images were acquired using 40-keV Ar_{4000}^+, and the analyzed area in the time-of-flight secondary ion mass spectrometry (ToF-SIMS) analysis was 4.8×4.8 mm^2. The crosses mark approximate locations of arterial ligation used to cause the infarction. Signal intensity for the ion images is displayed on a thermal scale, as shown on the right. Adapted with permission from Reference 55.

study of human breast cancer biopsy samples, Angerer et al. (56) correlated changes in phosphoinisitol lipid molecular ions with fatty acid fragment ions in different regions of the tumor itself and the surrounding stromal tissue. The secondary ion distributions of three different phosphoinisitol lipids with the same total number of carbon atoms but different degrees of unsaturation matched the distribution of three 20-carbon-containing fatty acid peaks [FA(20:2), FA(20:3), and FA(20:4)]. This suggested that the intact phosphoinisitol lipids of interest contained one equivalent acyl chain and one with FA(20:*x*), as shown in **Figure 4**, along with two colocalizing PC-lipid peaks detected in positive ion mode. The SIMS images were compared with H&E stained, consecutive tissue slices. Although the FA(20:2)- and FA(20:3)-containing phosphoinisitol lipids were associated with the tumor itself, the FA(20:4) signals were shown to be localized to regions of the stroma around the tumor where there were significant numbers of inflammatory cells.

Another recent and interesting use of peaks in the SIMS data besides the (pseudo)molecular ions comes from research by Sjövall's group (57). Similar to work from Szakal and colleagues (58), who showed that it was possible to assign secondary ions to nanoparticles based on the formation of metal cluster secondary ions, this recent lipid study reports the use of the phospholipid cluster ions (dimers in this case) in the SIMS spectrum to infer information about the local lipid environment at the point of the primary ion impact. This is based on the assumption that dimer formation between different lipids cannot occur once the secondary ions have reached the gas phase.

Although a major goal of SIMS development is to reduce the fragmentation of molecules during the sputtering process, careful analysis of the fragmentation products in the spectra and images can provide additional useful information.

IMPROVING IDENTIFICATION WITH NEW MASS ANALYZERS

Although inferences of lipid identities can be made by looking at fragment/(pseudo)molecular ion colocalization, such endeavors are greatly facilitated by improved mass spectrometer performance.

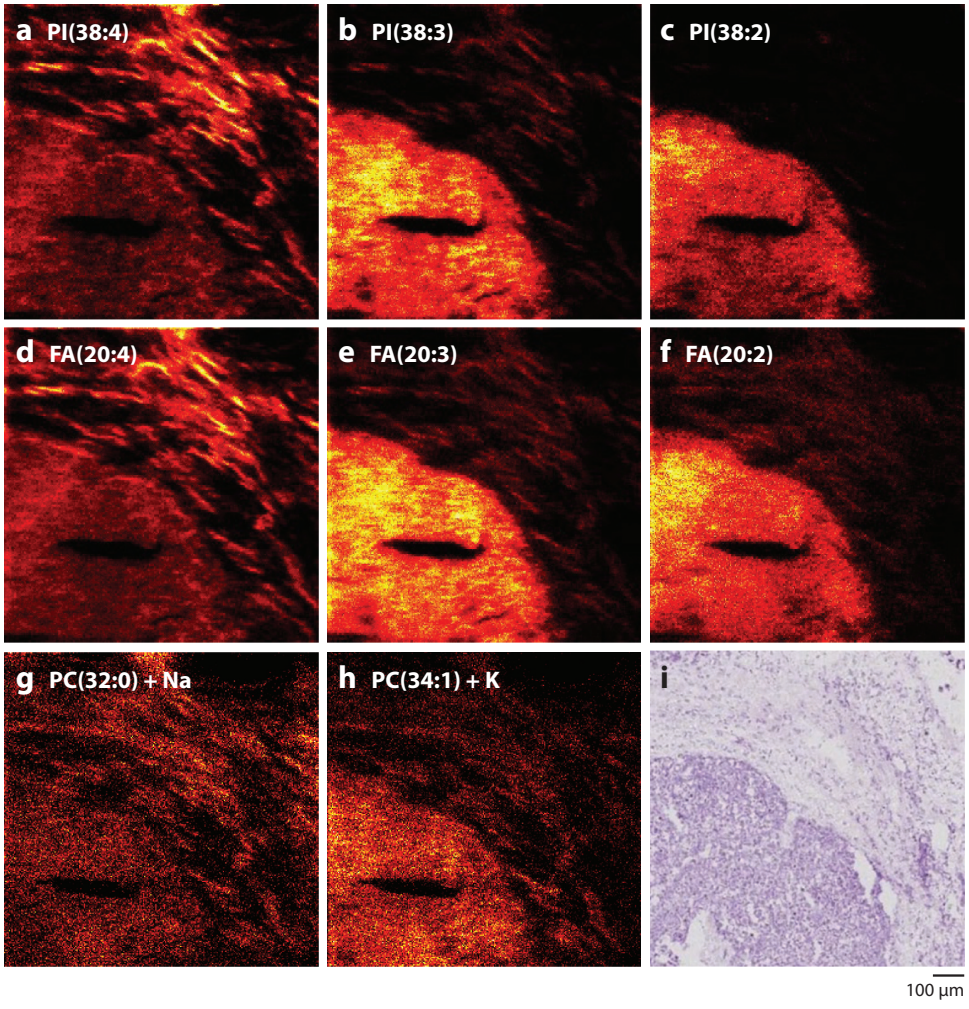

Figure 4

Secondary ion mass spectrometry (SIMS) imaging of intact lipid and colocalized fatty acid signals in human breast cancer tissue compared with conventional H&E staining. Single ion images at 3.9 µm/pixel show the intensity and distribution of $[M\text{-}H]^-$ ions of (*a*) PI(38:4), (*b*) PI(38:3), (*c*) PI(38:2), (*d*) FA(20:4), (*e*) FA(20:3), and (*f*) FA(20:2) imaged in negative ion mode and (*g*) $[PC(32:0)+Na]^+$ and (*h*) $[PC(34:1)+K]^+$ detected in positive ion mode. (*i*) H&E stained microscopy image of consecutive tissue section #9 showing cancerous (*purple*, *bottom left*) and inflammatory cell–containing stroma tissue (*brighter areas to top and right*). Adapted with permission from Reference 56. Copyright 2016, American Chemical Society.

Since the 1980s, many ToF-SIMS instruments have been designed to maximize transmission. While this provides advantages, particularly in the analysis of monolayer samples or very small quantities of analyte, it has been at the expense of mass accuracy, sometimes mass resolution, and the ability to perform tandem mass spectrometry (MS/MS) analysis. In a conventional ToF-SIMS experiment, the width of the peak in the mass spectrum is directly coupled to the width of the primary ion beam pulse. This is also influenced by sample topography and sample charging that can alter the energy of the secondary ions that are generated and, more subtly, by the partitioning of the energy in the ion as it is sputtered with molecules, atoms, and aromatics displaying different

peak shapes. There have been several approaches to improving mass resolution and accuracy in SIMS analysis. The use of delayed extraction where the secondary ion extraction is delayed to follow the primary ion pulse as opposed to occurring simultaneously is common in MALDI-ToF analysis. It has also been used in ToF-SIMS by a number research groups since the mid-2000s, especially on topographically challenging samples and when using ion beams with which very short pulses are difficult to produce (e.g., C_{60}^+) (17, 59).

More complex approaches have involved modification of the ion sources of existing mass spectrometry instruments to incorporate an ion gun for SIMS analysis. Carado et al. (60) initially added a C_{60}^+ ion beam to a Q-Star (AB Sciex LLC) instrument, which demonstrated the potential of such an approach for improving mass spectral quality. A modified version of this design has been used by Sweedler and coworkers (61).

Heeren and collaborators (62) also added a C_{60}^+ ion gun to a Fourier transform ion cyclotron resonance (FT-ICR) mass spectrometer (Bruker Corp.) and demonstrated the ability to generate SIMS spectra with very high mass resolution and mass accuracy. Both of these instrumental adaptations also included MS/MS capabilities that were features of the existing mass spectrometer platform but not available on any commercial SIMS instrument at the time.

In 2008, Vickerman and coworkers (63) reported initial data from a dedicated SIMS instrument that had been developed with biological analysis as a major target. It incorporated cryogenic sample handling with a glovebox entry system and featured a buncher-ToF mass analyzer that decoupled the mass spectrometry from the ion generation process so that mass resolution and accuracy were no longer affected by ion beam pulsing or the physical and electronic state of the sample. MS/MS is also provided by colliding the secondary ions with a collision gas between the buncher and the ToF mass analyzer. Originally designed to capitalize on the polyatomic ion beams such as C_{60}^+, the resulting J105 instrument (Ionoptika Ltd.) is well suited to use the more recent GCIBs. This instrument negates the requirement of very short primary ion pulses that are difficult to generate from GCIBs to achieve good mass resolution. Other SIMS instrument vendors have gradually introduced some of these features in their products. The nano-ToF II (Physical Electronics, Inc.) instrument incorporates an innovative MS/MS capability in that the MS/MS spectrum can be collected in parallel with the standard mass spectrum by pulsing out the mass window of interest for collisional activation and sending these resulting product ions down a second flight tube (64). Most recently, the National Physical Laboratory in the United Kingdom initiated the combining of an Orbitrap mass spectrometer (Thermo Fisher Scientific) with a ToF-SIMS 5 (IONTOF GmbH) to create the 3D OrbiSIMS (65). In this instrument, ions can be either sent into the ToF analyzer as normal or directed out of the normal SIMS instrument and into a connected Orbitrap instrument. Short ion beam pulsing is not required in Orbitrap mode, and GCIB analysis is facilitated as on the J105 instruments.

The addition of MS/MS capabilities to SIMS analysis has obvious benefits for structural elucidation and has been utilized in several studies. However, it is not as common as it is in LC-MS analysis of lipid extracts, for example, in part due to the lower signal levels of the secondary ions in the SIMS analysis. One advantage of MS/MS is that although SIMS analysis can produce some specific ions due to the high-energy processes occurring at the point of impact of the primary ion with the sample, intact molecular type ions that do survive generally produce product ions in MS/MS that match those from more common mass spectrometry, such as electrospray ionization and MALDI. Hence, MS/MS spectra from SIMS can be matched with MS/MS data from other mass spectrometry methods that are available in online databases (66).

However, some secondary ion types often observed in SIMS analysis of biological samples are not similar to those detected by softer ionization methods. Specifically, DAG-type ions are

often detected between *m/z* 400 and 700. Often casually assigned as DAG ions, the origin of these DAG-type peaks is actually unlikely to be DAGs, as these are often present only in low abundance and more likely to be generated from the fragmentation of other larger species during the ion ejection/formation process. Phan et al. (67) compared MS/MS spectra acquired on a J105 instrument to DAG and triaclglyceride (TAG) standards. The TAGs showed very low signals for the intact species but strong signals for the $[M\text{-}RCOO]^+$ ions that are isobaric with the $[M+H\text{-}H_2O]^+$ ions of DAGs. MS/MS of the *m/z* 551 ion from both tripalmitate and dipalmitate reference samples produced ions corresponding to RCO^+ and $[RCO+128]^+$. However, a notable difference was observed in the intensity of $[RCO+74]^+$ ion that was approximately 50% the intensity of the RCO^+ ion in the dipalmitate spectrum but was barely visible in the tripalmitate spectrum. The $[RCO+74]^+$ ion as a discriminator between DAG and TAG species was then used to assign several DAG-type ions in *Drosophila melanogaster* brain images originating from TAGs. Interestingly, in a recent SIMS/MALDI study of arteries undergoing restenosis, MS/MS of an ion assigned as the $[M+H\text{-}H_2O]^+$ ion of DAG(34:2) at *m/z* 575.5 on the nano-ToF II instrument produced the RCO^+ product ions but did not show the $[RCO+74]^+$ or the $[RCO+128]^+$ product ions. This suggested that, although both the J105 and nano-ToF II employ high-energy collision-induced association, there may be additional subtleties in the operation of the instruments that influence the product ions detected (68). In the absence of MS/MS capabilities, Sämfors et al. (69) have also reported that inspection of salt adduct formation can aid in assigning DAG-type ions to DAG or TAG species. Whereas DAGs readily form $[M+Na]^+$ ions, TAGs do not fragment to produce isobaric ions.

Improvements in mass accuracy from approximately 150 ppm for conventional ToF-SIMS to approximately 5 ppm on the J105 instrument provide advantages for putative assignment of lipid species. However, to increase the diversity of lipid signals detected, high mass accuracy sometimes needs to be coupled with corresponding high mass resolution. Merging the Orbitrap analyzer to the ToF-SIMS instrument on the 3D OrbiSIMS provides this capability, albeit with a significant sacrifice in analysis time. In the supporting information of the initial demonstration paper of their hybrid instrument, Passarelli et al. (65) provide a list of the different lipid species detected using the Orbitrap mass analyzer operating at a mass resolution, $m/\Delta m$, of 240,000 (compared with the ~10,000 normally reported on biological samples analyzed by ToF-SIMS) from the hippocampus of mouse brain. Most potential isobaric interferences are reported in negative ion mode where several phosphatidylethanolamine species occur at the same nominal mass as sulfatide peaks. However, these interferences are separated by approximately 0.05–0.07 Da and thus have the potential to be resolved on a ToF analyzer. The performance of the FT-MS really provides advantages for resolving isobaric interference when changes in saturation need to be resolved from ^{13}C isotopes of other species. Because most of the lipids show multiple degrees of saturation, this problem is much more common. The presence of the different species can be detected on a ToF analyzer and the relative abundances calculated from predicted isotope ratios. However, as the mass difference is only approximately 0.015 Da (2 neutrons versus 2 hydrogen atoms), resolving the different species on a normal ToF mass analyzer is not realistic, which will affect imaging of the different ions because one of the overlapping species will appear as chemical/background noise in the image of the other.

Hence, it is an exciting time for instrument development for SIMS. Development of new mass analyzers has been an important step toward improving the SIMS technique for analysis of lipids in biological samples. The ability to accurately identify various lipid species and differentiate them from overlapping isobaric interfering peaks makes the technique better suited for studies of lipids and other samples.

SAMPLE PREPARATION FOR LIPID IMAGING WITH SIMS

As with most analytical techniques, sample preparation is critical to the acquisition of meaningful data. As such, a range of approaches has been proposed and demonstrated to improve the preservation of a lifelike state by minimizing chemical redistribution of the analytes as the sample is introduced to the high vacuum environment of the SIMS instrument. There have also been studies in which sample preparation has focused on increasing the signals from either specific analytes or classes of molecules to increase the diversity of the chemical coverage of the analysis. Some of the preparation approaches have been borrowed from the electron microscopy field, particularly the use of in vacuo freeze fracture. Here, cells are sandwiched between two suitable slices of typically silicon or steel, plunged frozen in a suitable cryogen such as isopentane or liquid propane to minimize ice crystal formation and transferred to the vacuum of the instrument where the sandwich is prized apart, presenting a pristine frozen surface. Such an approach was used for preparation of the *Tetrahymena*, shown in **Figure 1**, and various semi-automated in vacuo freeze fracture solutions have been demonstrated for different SIMS instruments (45, 70, 71).

Rodent brain sections are a common sample for imaging mass spectrometry, and imaging SIMS is no exception. The challenge related to cholesterol masking other lipid signals in the white matter region has been the focus of a number of studies where different sample preparation methodologies have been employed to overcome this.

The gold standard approach is to maintain the sample in a hydrated state at cryogenic temperatures during analysis. Unfortunately, this approach is not always possible or practical. Tissue slicing may not always be performed in the mass spectrometry laboratory, and so maintaining frozen samples during transport to the analysis lab and into the instrument without significant exposure to water vapor can be very difficult. Further, many SIMS instruments do not have suitable cold sample handling capabilities. Hence, alternative methods to overcome the cholesterol issue have been proposed, such as exposure to reactive vapors, including trifluoroacetic acid (TFA) or ammonia. The spectra from the white matter region of rat brain before and after exposure to TFA (30 min in a desiccator at room temperature) are shown in **Figure 5*a***. While the freeze-dried tissue spectrum is dominated by signals from cholesterol (the intense black peak at *m/z* 369 in **Figure 5*a***), including the dimer and trimer ions, a rich lipid spectrum (see intact lipid region between *m/z* 700 and 900 in **Figure 5*a***) is obtained following the TFA treatment, where scanning electron microscope (SEM) analysis indicated the removal of small, suspected cholesterol crystals from the surface of the tissue. The difference in the secondary ion intensity distributions of PC(34:1) and $[M+K]^+$ (*m/z* 798.5) ion in control-vacuum-desiccated brain and following TFA exposure is also clearly evident in the mouse cerebellum tissue shown **Figure 5*b*** and **Figure 5*c***, respectively. A follow-up study, focused on negative ion mode signals, compared signals from the hippocampus of rat brain when analyzed in frozen-hydrated (**Figure 5*d***) or freeze-dried (**Figure 5*e***) conditions and after the freeze-dried tissue had been exposed to ammonia vapor (NH_3) (**Figure 5*f***). Signal loss following freeze drying is recovered somewhat by the exposure to ammonia vapor (73).

Frozen hydrated analysis may also be required when samples contain particularly mobile species, as reported in the analysis of sectioned *D. melanogaster* heads where mobile lipids detected as DAG-type ions migrated across the brain regions of interest from the proboscis region. Lee and coworkers (74) have demonstrated that this migration may be ameliorated if tape mounting, as opposed to the general practice of thaw mounting the tissue sections, is used because this reduces tissue shrinkage and deformation during drying. In a more advanced example of sample pretreatment for SIMS, Tian et al. (75) employed a chemical and biological tissue treatment protocol previously developed for MALDI analysis to improve the detection of low-abundance cardiolipins in rodent brain sections. The treatment uses 1-ethyl-3-[3-(dimethylamino)propyl] carbodiimide

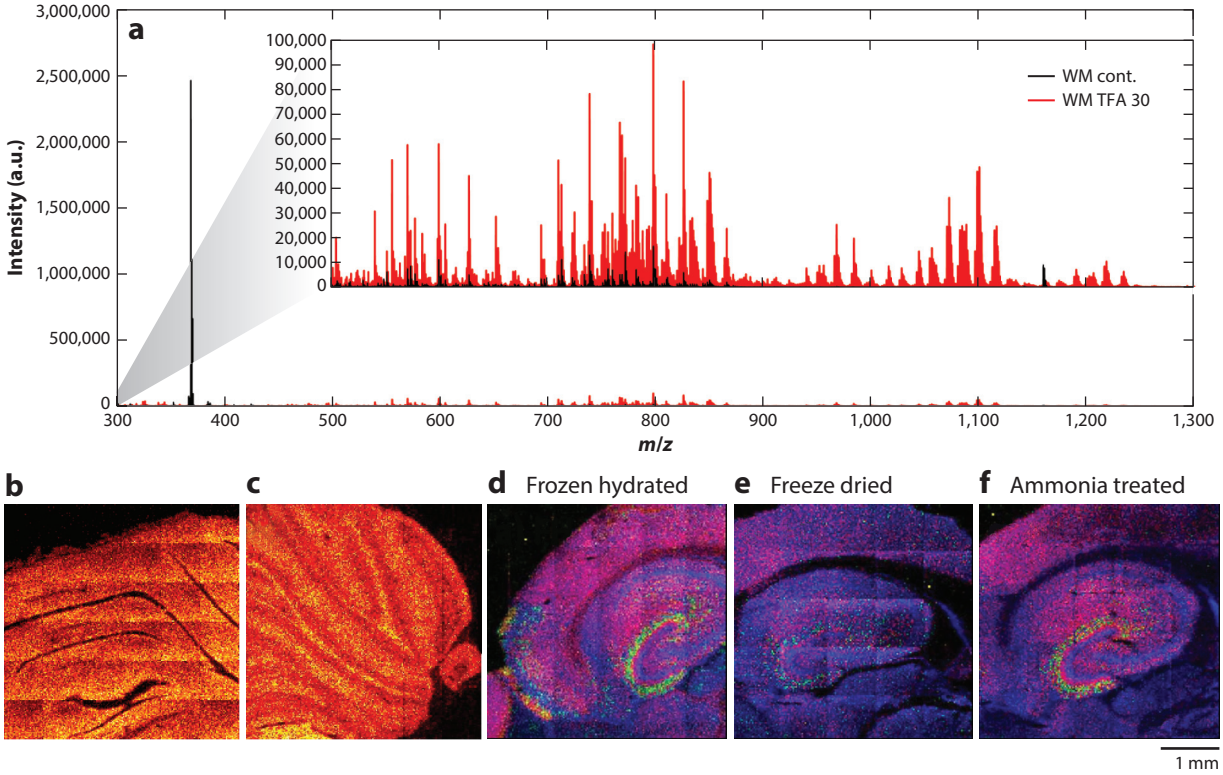

Figure 5

(*a*) Differences in the time-of-flight secondary ion mass spectrometry (ToF-SIMS) spectra from the white matter region in rat brain between control (WM Cont.) tissue, shown in black, and tissue following a 30-min exposure to trifluoroacetic acid (TFA) vapor (WM TFA 30), shown in red. Panel created by replotting of some data included in Reference 72. The control spectrum is dominated by a cholesterol signal at *m/z* 369 with relatively low lipid signal compared to the TFA-exposed tissue that shows mainly phospholipid species, particularly in the *m/z* 700–900 range. Distribution of PC(34:1), $[M+K]^+$ (*m/z* 798.5) in control and TFA-exposed tissue (panels *b* and *c*, respectively). Adapted with permission from Reference 72. Copyright 2015, American Chemical Society. ToF-SIMS images comparing (*d*) frozen-hydrated, (*e*) freeze-dried, and (*f*) ammonia-treated samples, with a focus on two brain areas, the isocortex and molecular layer. The peaks used to generate the red-green-blue overlay images are *m/z* 885.5 PI(38:4) $[M-H]^-$, *m/z* 1544.9 GM1 (36:1) $[M-H]^-$, and *m/z* 1572.9 GM1 (38:1) $[M-H]^-$. All data were acquired using 40-keV Ar_{4000}^+, ion dose: 1×10^{12} ions/cm^2, negative ion mode. Adapted with permission from Reference 73.

hydrochloride (EDC) and phospholipase C (PLC), removes the abundant phosphatidylcholines, and allows the cardiolipins to be imaged at 8-μm spatial resolution within the tissue section (76). Using this EDC/PLC approach, researchers observed the depletion of cardiolipin signal in injured rat brain regions following controlled traumatic brain injury by pneumatically driven impact to the left parietal cortex.

EMERGING RESEARCH DIRECTIONS

Bacterial Membranes

SIMS has been used in several studies where multivariate analysis of the data has been used for classification of different species and strains of bacteria. The surface-sensitive analysis has also been shown to be useful for detecting secreted signaling molecules and defensive antibiotics and

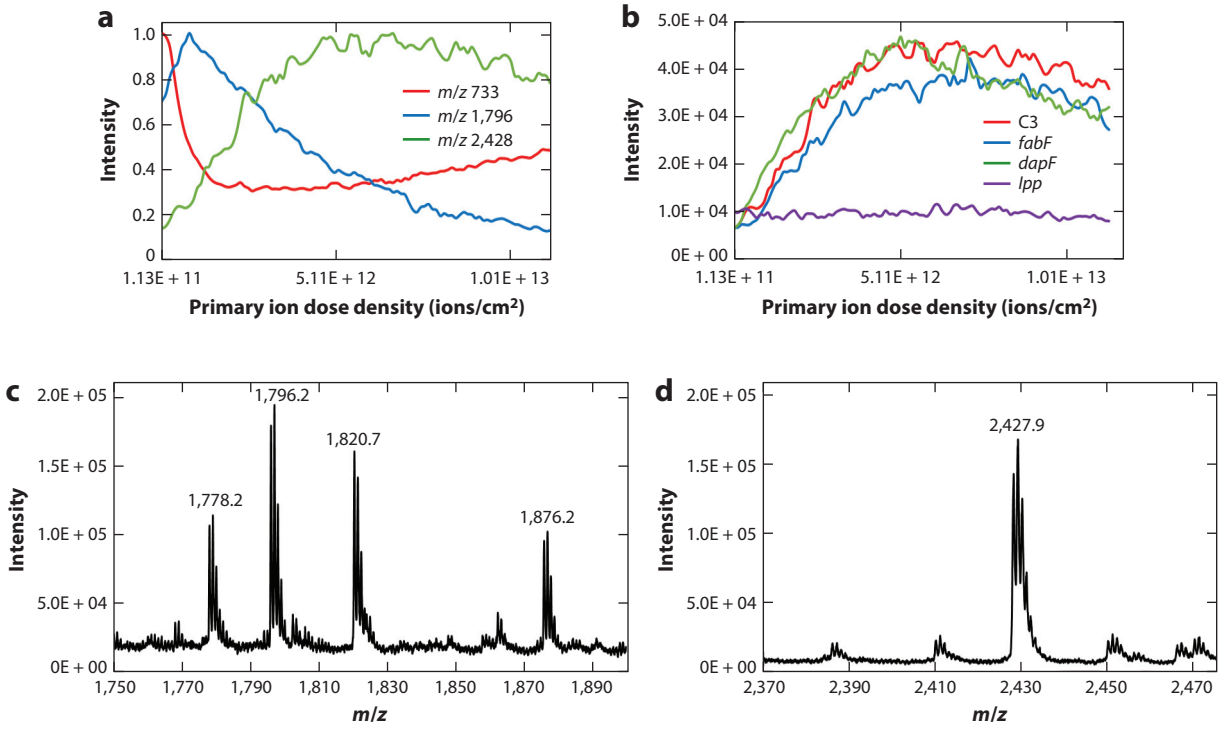

Figure 6

(*a*) Depth profiles of PG(cp33:0) at *m/z* 733, lipid A at *m/z* 1,796, and ECA_{CYC} at *m/z* 2,428 showing the different signal profiles of these species in *Escherichia coli*. (*b*) Depth profile of *m/z* 2,428 illustrating the difference in signal and comparing a control sample and 3 mutants (*fabF* and *dapF* to *lpp*). Note that the ECA_{CYC} signal from the *lpp* mutant does not appear as the sample is depth profiled. (*c*) Excerpt of the mass spectrum from analysis of the control *E. coli* sample showing the isotopic mass and isotopic pattern of lipid A at *m/z* 1,796 (Δ 11 ppm), *m/z* 1,820 (suspected ECA_{CYC} fragment ion), and surrounding species. (*d*) Excerpt of the mass spectrum from the analysis of control *E. coli* sample showing the isotopic mass and isotopic pattern of *m/z* 2,428 putatively assigned as ECA_{CYC}. Adapted from Reference 81. Copyright 2019, American Chemical Society.

studying lipid changes associated with the stringent response (77–80). In a recent study of the membrane composition of different *Escherichia coli* mutants known to have impaired plasmid transfer capabilities, Nilsson et al. (81) reported characteristic lipid changes observed in different regions of the mass spectra. This was particularly relevant to cyclopropane-containing fatty acids, the intact phospholipid *m/z* region of the mass spectra, and the cardiolipin mass range (approximately 1300–1500 Da.), which again highlights the improved coverage of different lipid sizes afforded by the GCIBs. Notably, in this recent study, the GCIB—a 40-keV $(CO_2)_{6k}^+$ beam—was used to erode the bacterial envelope and in doing so uncovered even larger lipid species below the surface: specifically, lipid A and cyclic enterobacterial common antigen (ECA_{CYC}) at *m/z* 1,796 and 2,428, respectively. **Figure 6** shows a plot of variation in signal intensity of three different lipid species as the bacterial envelope was eroded. Although the exact erosion depth is not known, the estimated depth is approximately 50 nm based on known erosion rates through organic layers. The very surface of the bacteria shows high signals for *m/z* 733 assigned to PG(cp33:0). Lipid A, the component of the lipopolysaccharide (LPS) on the coating of gram-negative bacteria that is responsible for anchoring the LPS to the outer membrane, is detected at *m/z* 1,796. Lipid A is a major constituent of the bacterial lipid membrane, whereas ECA_{CYC}, detected at *m/z* 2,428, is

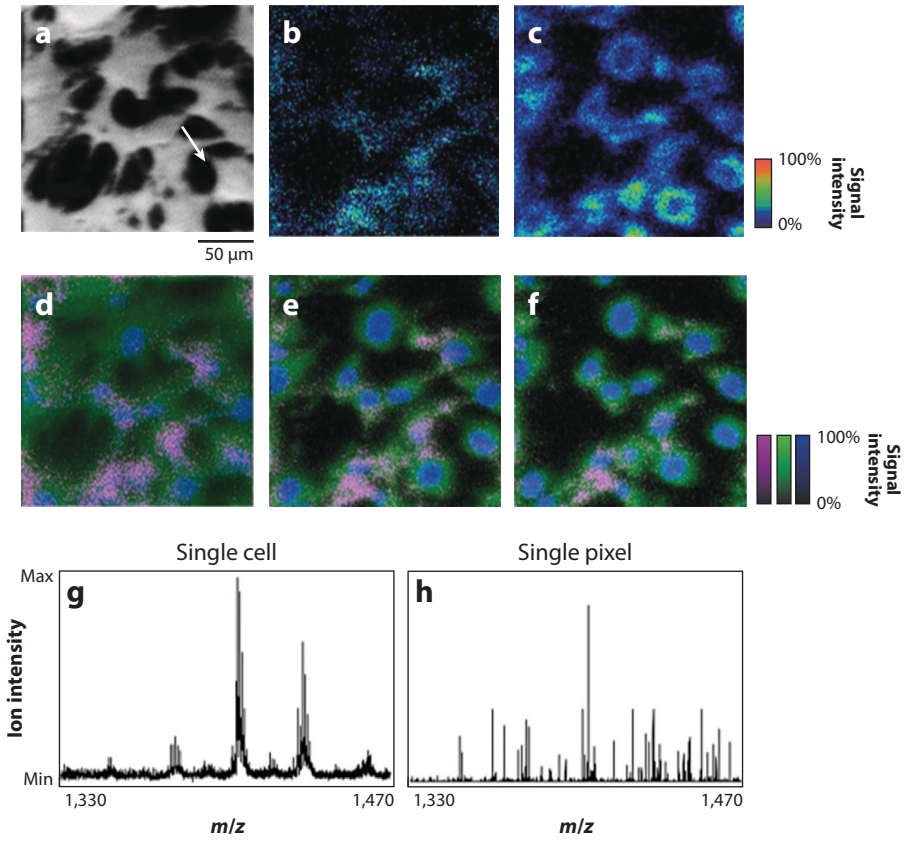

Figure 7

Gas cluster ion beam-secondary ion mass spectrometry (GCIB-SIMS) imaging of hippocampal neuronal HT22 cells, treated with (1-ethyl-3-(3-dimethylaminopropyl)carbo- diimide hydrochloride) and phospholipase C prior to analysis for enhancement of cardiolipin (CL) signals. Images were captured at 1 µm per pixel. (*a*) Total ion image of the first layer showing the outline of the cells (*white arrow* pointing to a cell). Second-layer SIMS images show (*b*) the *m/z* 1,404.0 peak identified as CL(68:2) and (*c*) the *m/z* 885.5 peak identified as PI(38:4), illustrating subcellular structures. (*d–f*) Panels show overlay images of depth profiling of cells at different depths in the sample. Green, PI(38:4); blue, deoxyribose phosphate (*m/z* 257.0); magenta, CL(68:2). (*d*) First layer (0–200 nm), (*e*) second layer (200–400 nm), and (*f*) third layer of the profile (400–600 nm). (*g*) SIMS spectrum from the first layer of the single cell indicated in panels *a* and *h* is from a representative single pixel within that cell. Adapted with permission from Reference 82.

expected to reside in the periplasm between the inner and outer lipid membranes of the bacteria. These results present new avenues for SIMS analysis because the remarkably high surface sensitivity and depth resolution of the technique provide the chemical location of the different lipids and not the focus of the ion beam.

In this study (81), small droplets of many bacteria were analyzed as opposed to single cells. The goal of SIMS for lipidomics is to transfer the increasing sensitivity to lipids and diversity of lipids detected to subcellular imaging. Unfortunately, GCIBs are much more difficult to focus than liquid metal and even C_{60} ion beams. However, recent work from the Winograd lab (82) has utilized a higher-energy (70-keV) GCIB to perform 3D imaging of lipids in single cells (**Figure 7**). Hippocampal neuronal HT22 cells were imaged with a pixel size of 1 µm following the

same EDC/PLC treatment used to improve cardiolipin signal in the traumatic brain injury study mentioned above. Notable is the move away from the use of small fragments to image the lipid membrane, as this is now displayed using the intact PI(38:4) $[M\text{-}H]^+$ signal. The cardiolipin was expected to be specific to the mitochondria, thus demonstrating the potential for SIMS imaging to begin imaging molecules with organelle specificity.

Water Beams

Although GCIBs have greatly improved the detection of intact lipid ions, there is still a demand for improved ionization and increased sensitivity in SIMS analysis. One recent direction is to switch from inert gas clusters to reactive gas clusters. Of particular note for lipid analysis is the gradual introduction of water cluster ion beams (83–85). Increased secondary ion signals have been shown through the interaction of water ice, water vapor above cold samples, and higher-pressure water vapor at room temperature (86–88). Hence, incorporating this enhancement ability into the ionizing beam itself offers the potential to provide a more elegant solution to low ionization efficiency by providing a potential source of protons at the point of impact. Several recent reports suggest a potentially several-orders-of-magnitude increase in secondary ion signal when water cluster beams are used, providing that the energy per constituent H_2O in the cluster is in the optimal range. This has been shown experimentally to be between 2 and 5 eV. Although the initial expectation was that the water would act as a proton source for secondary ion formation, recent work by Sheraz and coworkers (89) demonstrates that secondary ion signal enhancement is also achieved for negative ions. Combining the water cluster source with a 70-keV gas cluster ion gun allowed subcellular imaging to be performed using the water clusters. The greatest relative signal increases came from cardiolipin peaks that were enhanced 100–500× when analyzed in frozen hydrated samples with a water cluster beam compared with chemically fixed cells analyzed at room temperature with a CO_2 gas cluster beam. 3D cardiolipin imaging is now possible in cells without the EDC/PLC treatment previously employed (see sidebar titled NanoSIMS).

TARGETED ANALYSIS BY ISOTOPIC LABELING

Although the previous discussions and examples have emphasized the growing capabilities of SIMS analysis for probing the diversity of lipid species, there are specific applications where the

NanoSIMS

Biological imaging using magnetic sector SIMS has been used since the 1970s. Analysis using these dynamic SIMS instruments is limited to atomic/elemental species or very small fragment ions, with reports focusing on the distribution of Na, K, Ca, and B (from boron neutron capture therapy, BNCT, or drugs) (90–94). The nanoSIMS is a dynamic SIMS instrument available from Cameca Ametek capable of 50-nm-resolution imaging and the detection of 7 species simultaneously; it also provides very sensitive isotope measurements at high spatial resolution. Often it is not ion abundance that is displayed in an image but instead the relative enrichment of a specific isotope. Lechene at Harvard (95) pioneered the use of multi-isotope imaging mass spectrometry (MIMS) to study localized protein turnover in 2D and 3D. The instrument has also been used to study Pt containing anticancer drugs and lanthanide tagged antibodies (96, 97). Extensive sample preparation close to that used for transmission electron microscopy is often used to reach the ultimate spatial resolution of the instrument. Owing to the unique approaches to sample preparation and analysis, nanoSIMS is often referred to as an analytical technique itself and not used solely as the name given to the instrument by the vendor.

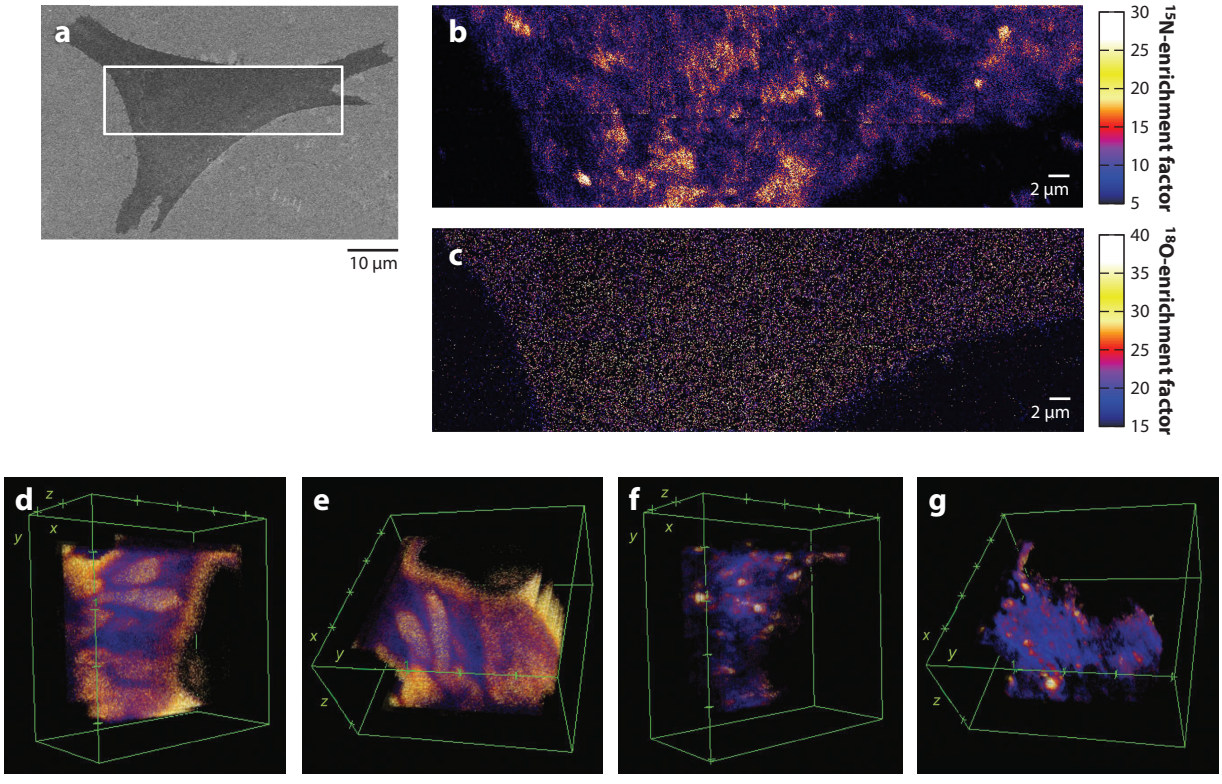

Figure 8

(*a*) Scanning electron microscopy (SEM) image of a clone 15 cell. The approximate location that was analyzed with high-resolution secondary ion mass spectrometry (SIMS) is outlined. (*b*) The distribution of metabolically incorporated ^{15}N-sphingolipids in the plasma membrane of the cell was imaged by detecting the sphingolipid-specific ^{15}N enrichment with high-resolution SIMS. Orange and yellow regions represent plasma membrane domains that are enriched with ^{15}N-sphingolipids. (*c*) Mosaic of ^{18}O-enrichment images acquired with high-resolution SIMS shows that the metabolically incorporated ^{18}O-cholesterol is relatively uniformly distributed in the plasma membrane. Adapted with permission from Reference 98. Three-dimensional (3D) renderings of the ^{18}O-cholesterol and ^{15}N-sphingolipid distributions in an approximately 2.3-µm-thick region in an MDCK cell were created by stacking 61 isotope enrichment images acquired over 24 h. Each of the 61 images in the stack consists of data from ten raster planes. These images were aligned to correct for the sample and stage drift that occurred during the experiment, and a transparency of 50% was applied for better visualization. The 3D renderings were not adjusted to compensate for surface topography or potential changes in the sputter rate within the cell. Side (*d*) and top (*e*) views of the 3D rendering of the ^{18}O enrichment show that ^{18}O-cholesterol is concentrated in tubular projections that span the analysis depth. A combination of image alignment for drift correction and the 50% transparency gives the appearance of curvature along the *z*-axis (*top left* of panel *d* and *bottom left* of panel *e*). Side (*f*) and top (*g*) views of the 3D distribution of ^{15}N enrichment show smaller pockets of ^{15}N-sphingolipids that do not correlate with the ^{18}O-rich regions. Adapted with permission from Reference 99.

diversity is sacrificed for specificity and/or spatial resolution. Most lipid analysis with SIMS is performed using a ToF analyzer, with the notable exceptions of the FT-ICR and Orbitrap examples mentioned previously. However, through the introduction of isotopic labels to different lipids, Kraft and coworkers (98, 99) have used a nanoSIMS magnetic sector instrument (Cameca Ametek) to study lipid organization in cell membranes. The research demonstrated that, contrary to the hypothesis, cholesterol and sphingolipids did not localize to the same membrane lipid domains. **Figure 8** shows SEM and nanoSIMS images of ^{18}O-labeled cholesterol and ^{15}N-labeled

sphingolipids in the membrane of a fibroblast cell (**Figure 8*a–c***) and the 3D renderings of the same signals from the 3D SIMS analysis of a Madin-Darby canine kidney (MDCK) cell (**Figure 8*d–g***).

Isotopic labeling of lipids does not have to be limited to nanoSIMS analysis. Phospholipids labeled with deuterium have been followed as they incorporate into the cell membrane of PC12 cells, in this case looking at the deuterated fragments from the lipids, and the effect of the change of lipid composition on exocytosis was studied (100). More recently, PC12 cells were incubated with isotopically labeled essential fatty acids, omega-3 and omega-6. ToF-SIMS was then used to track the incorporation of these fatty acids into the cell membrane using the fatty acid ions and intact lipid signals, aided by the use of a GCIB primary ion beam (101). Both the omega-3 and omega-6 were found to mainly incorporate into phosphatidylcholine, phosphatidylethanolamine, and phosphatidylinositol species, and relative quantification of the lipid species showed that the omega-3 fatty acids are incorporated in higher amounts than omega-6 fatty acids.

CONCLUSIONS

Lipids represent important analytical targets, and although there are many powerful analytical methods for studying them, SIMS is uniquely placed for in situ analysis of these compounds, potentially on an organelle scale. The development of ion beams such as GCIBs has opened up the possibility of imaging intact lipid ions within cells, even in 3D. Continued developments in this area, such as the use of more reactive primary ion species including water, have the potential to improve sensitivity further. Multiple SIMS instrument vendors have now acknowledged the need to improve spectral quality and the benefit of features such as MS/MS. This rapid development in instrument capabilities is already having a large impact on the detection and identification of lipid species in SIMS experiments.

As an overall technique, SIMS offers ultimate spatial resolution on the order of tens of nanometers, and while intact lipid detection may be difficult on this scale, the use of targeted approaches such as the isotopic labeling common to nanoSIMS analysis allows subcellular features to be imaged in 3D.

For broad coverage of diverse lipid types of different sizes, the development of GCIBs, including new reactive GCIBs such as water cluster ion beams, has provided huge gains. The softer secondary ion generation process increases the proportion of intact lipid ions generated and has allowed lipids with masses over 1,000 Da to be imaged in single cells.

The advances and increasing diversity of the mass analyzers used for SIMS analysis are allowing the full potential of the GCIBs to be harnessed. They also improve the ability to more specifically identify different lipids through improved mass resolution and accuracy and MS/MS capabilities.

The improvements in sensitivity and spectral quality combine to increase the diversity of lipid species that can be detected and confidently assigned. This just leaves the final, great challenge of quantitation!

DISCLOSURE STATEMENT

The authors are not aware of any affiliations, memberships, funding, or financial holdings that might be perceived as affecting the objectivity of this review.

ACKNOWLEDGMENTS

The authors gratefully acknowledge financial support from the Swedish Research Council (VR) and the University of Gothenburg.

LITERATURE CITED

1. Singer SJ, Nicolson GL. 1972. The fluid mosaic model of the structure of cell membranes. *Science* 175:720–31
2. Fahy E, Subramaniam S, Brown H, Glass C, Merrill A Jr., Murphy R, et al. 2005. A comprehensive classification system for lipids. *J. Lipid Res.* 46:839–62
3. Fahy E, Subramaniam S, Murphy RC, Nishijima M, Raetz CR, et al. 2009. Update of the LIPID MAPS comprehensive classification system for lipids. *J. Lipid Res.* 50:S9–14
4. Harayama T, Riezman H. 2018. Understanding the diversity of membrane lipid composition. *Nat. Rev. Mol. Cell Biol.* 19:281–96
5. Yeagle PL. 1985. Cholesterol and the cell membrane. *Biochim. Biophys. Acta* 822:267–87
6. Coskun Ü, Simons K. 2011. Cell membranes: the lipid perspective. *Structure* 19:1543–48
7. Van Meer G, Voelker DR, Feigenson GW. 2008. Membrane lipids: where they are and how they behave. *Nat. Rev. Mol. Cell Biol.* 9:112–24
8. Murata N, Los DA. 1997. Membrane fluidity and temperature perception. *Plant Physiol.* 115:875–79
9. Martin CE, Hiramitsu K, Kitajima Y, Nozawa Y, Skriver L, Thompson GA Jr. 1976. Molecular control of membrane properties during temperature acclimation. Fatty acid desaturase regulation of membrane fluidity in acclimating *Tetrahymena* cells. *Biochemistry* 15:5218–27
10. Shevchenko A, Simons K. 2010. Lipidomics: coming to grips with lipid diversity. *Nat. Rev. Mol. Cell Biol.* 11:593–98
11. Rouser G, Fleischer S, Yamamoto A. 1970. Two dimensional thin layer chromatographic separation of polar lipids and determination of phospholipids by phosphorus analysis of spots. *Lipids* 5:494–96
12. Christie WW. 1985. Rapid separation and quantification of lipid classes by high performance liquid chromatography and mass (light-scattering) detection. *J. Lipid Res.* 26:507–12
13. Morita S, Terada T. 2015. Enzymatic measurement of phosphatidylglycerol and cardiolipin in cultured cells and mitochondria. *Sci. Rep.* 5:11737
14. Kuerschner L, Moessinger C, Thiele C. 2008. Imaging of lipid biosynthesis: how a neutral lipid enters lipid droplets. *Traffic* 9:338–52
15. Schütz GJ, Kada G, Pastushenko VP, Schindler H. 2000. Properties of lipid microdomains in a muscle cell membrane visualized by single molecule microscopy. *EMBO J.* 19:892–901
16. Passarelli MK, Ewing AG, Winograd N. 2013. Single-cell lipidomics: characterizing and imaging lipids on the surface of individual *Aplysia californica* neurons with cluster secondary ion mass spectrometry. *Anal. Chem.* 85:2231–38
17. Fletcher JS, Lockyer NP, Vaidyanathan S, Vickerman JC. 2007. TOF-SIMS 3D biomolecular imaging of *Xenopus laevis* oocytes using buckminsterfullerene (C_{60}) primary ions. *Anal. Chem.* 79:2199–206
18. Tian H, Fletcher JS, Thuret R, Henderson A, Papalopulu N, et al. 2014. Spatiotemporal lipid profiling during early embryo development of *Xenopus laevis* using dynamic ToF-SIMS imaging. *J. Lipid Res.* 55:1970–80
19. Robinson MA, Graham DJ, Morrish F, Hockenbery D, Gamble LJ. 2016. Lipid analysis of eight human breast cancer cell lines with ToF-SIMS. *Biointerphases* 11:02A303
20. Ren L, Dowlatshahi Pour M, Malmberg P, Ewing AG. 2019. Altered lipid composition of secretory cells following exposure to zinc can be correlated to changes in exocytosis. *Chem. A Eur. J.* 25:5406–11
21. Munem M, Zaar O, Nilsson KD, Neittaanmaki N, Paoli J, Fletcher JS. 2018. Chemical imaging of aggressive basal cell carcinoma using time-of-flight secondary ion mass spectrometry. *Biointerphases* 13:03B402
22. Touboul D, Roy S, Germain DP, Chaminade P, Brunelle A, Laprévote O. 2007. MALDI-TOF and cluster-TOF-SIMS imaging of Fabry disease biomarkers. *Int. J. Mass Spectrom.* 260:158–65
23. Bruinen AL, Fisher GL, Heeren RMA. 2017. ToF-SIMS parallel imaging MS/MS of lipid species in thin tissue sections. In *Imaging Mass Spectrometry: Methods and Protocols*, ed. LM Cole, pp. 165–73. New York: Springer

24. Phan NTN, Fletcher JS, Ewing AG. 2015. Lipid structural effects of oral administration of methylphenidate in *Drosophila* brain by secondary ion mass spectrometry imaging. *Anal. Chem.* 87:4063–71
25. Angerer TB, Chakravarty N, Taylor MJ, Nicora CD, Graham DJ, et al. 2019. Insights into the histology of planarian flatworm *Phagocata gracilis* based on location specific, intact lipid information provided by GCIB-ToF-SIMS imaging. *Biochim. Biophys. Acta Mol. Cell Biol. Lipids* 1864:733–43
26. Tahallah N, Brunelle A, De La Porte S, Laprévote O. 2008. Lipid mapping in human dystrophic muscle by cluster-time-of-flight secondary ion mass spectrometry imaging. *J. Lipid Res.* 49:438–54
27. Touboul D, Brunelle A, Halgand F, De La Porte S, Laprévote O. 2005. Lipid imaging by gold cluster time-of-flight secondary ion mass spectrometry: application to Duchenne muscular dystrophy. *J. Lipid Res.* 46:1388–95
28. Davies N, Weibel DE, Blenkinsopp P, Lockyer N, Hill R, Vickerman JC. 2003. Development and experimental application of a gold liquid metal ion source. *Appl. Surf. Sci.* 203:223–27
29. Touboul D, Kollmer F, Niehuis E, Brunelle A, Laprévote O. 2005. Improvement of biological time-of-flight-secondary ion mass spectrometry imaging with a bismuth cluster ion source. *J. Am. Soc. Mass Spectrom.* 16:1608–18
30. Gunnarsson A, Kollmer F, Sohn S, Höök F, Sjövall P. 2010. Spatial-resolution limits in mass spectrometry imaging of supported lipid bilayers and individual lipid vesicles. *Anal. Chem.* 82:2426–33
31. Kurczy ME, Piehowski PD, Van Bell CT, Heien ML, Winograd N, Ewing AG. 2010. Mass spectrometry imaging of mating *Tetrahymena* show that changes in cell morphology regulate lipid domain formation. *PNAS* 107:2751–56
32. Ostrowski SG, Van Bell CT, Winograd N, Ewing AG. 2004. Mass spectrometric imaging of highly curved membranes during *Tetrahymena* mating. *Science* 305:71–73
33. Amaya KR, Monroe EB, Sweedler JV, Clayton DF. 2007. Lipid imaging in the zebra finch brain with secondary ion mass spectrometry. *Int. J. Mass Spectrom.* 260:121–27
34. Kezutyte T, Desbenoit N, Brunelle A, Briedis V. 2013. Studying the penetration of fatty acids into human skin by ex vivo TOF-SIMS imaging. *Biointerphases* 8:3
35. Debois D, Bralet M-P, Le Naour F, Brunelle A, Laprévote O. 2009. *In situ* lipidomic analysis of nonalcoholic fatty liver by cluster TOF-SIMS imaging. *Anal. Chem.* 81:2823–31
36. Cullen P, Fobker M, Tegelkamp K, Meyer K, Kannenberg F, et al. 1997. An improved method for quantification of cholesterol and cholesteryl esters in human monocyte-derived macrophages by high performance liquid chromatography with identification of unassigned cholesteryl ester species by means of secondary ion mass spectrometry. *J. Lipid Res.* 38:401–9
37. Lee ES, Shon HK, Lee TG, Kim SH, Moon DW. 2013. The regional ratio of cholesteryl palmitate to cholesteryl oleate measured by ToF-SIMS as a key parameter of atherosclerosis. *Atherosclerosis* 226:378–84
38. Lehti S, Sjövall P, Käkelä R, Mäyränpää MI, Kovanen PT, Öörni K. 2015. Spatial distributions of lipids in atherosclerosis of human coronary arteries studied by time-of-flight secondary ion mass spectrometry. *Am. J. Pathol.* 185:1216–33
39. McDonnell LA, Heeren RMA. 2007. Imaging mass spectrometry. *Mass Spectrom. Rev.* 26:606–43
40. Benabdellah F, Seyer A, Quinton L, Touboul D, Brunelle A, Laprévote O. 2010. Mass spectrometry imaging of rat brain sections: nanomolar sensitivity with MALDI versus nanometer resolution by TOF–SIMS. *Anal. Bioanal. Chem.* 396:151–62
41. Wu KJ, Odom RW. 1996. Matrix-enhanced secondary ion mass spectrometry: a method for molecular analysis of solid surfaces. *Anal. Chem.* 68:873–82
42. Sjövall P, Lausmaa J, Nygren H, Carlsson L, Malmberg P. 2003. Imaging of membrane lipids in single cells by imprint-imaging time-of-flight secondary ion mass spectrometry. *Anal. Chem.* 75:3429–34
43. Wong SCC, Hill R, Blenkinsopp P, Lockyer NP, Weibel DE, Vickerman JC. 2003. Development of a C_{60}^+ ion gun for static SIMS and chemical imaging. *Appl. Surf. Sci.* 203:219–22
44. Jones EA, Fletcher JS, Thompson CE, Jackson DA, Lockyer NP, Vickerman JC. 2006. ToF-SIMS analysis of bio-systems: Are polyatomic primary ions the solution? *Appl. Surf. Sci.* 252:6844–54

45. Fletcher JS, Rabbani S, Henderson A, Lockyer NP, Vickerman JC. 2011. Three-dimensional mass spectral imaging of HeLa-M cells—sample preparation, data interpretation and visualisation. *Rapid Commun. Mass Spectrom.* 25:925–32
46. Breitenstein D, Rommel CE, Stolwijk J, Wegener J, Hagenhoff B. 2008. The chemical composition of animal cells reconstructed from 2D and 3D ToF-SIMS analysis. *Appl. Surf. Sci.* 255:1249–56
47. Debois D, Brunelle A, Laprévote O. 2007. Attempts for molecular depth profiling directly on a rat brain tissue section using fullerene and bismuth cluster ion beams. *Int. J. Mass Spectrom.* 260:115–20
48. Fletcher JS, Lockyer NP, Vickerman JC. 2011. Molecular SIMS imaging; spatial resolution and molecular sensitivity: Have we reached the end of the road? Is there light at the end of the tunnel? *Surf. Interface Anal.* 43:253–56
49. Sjövall P, Johansson B, Lausmaa J. 2006. Localization of lipids in freeze-dried mouse brain sections by imaging TOF-SIMS. *Appl. Surf. Sci.* 252:6966–74
50. Yamada I, Matsuo J, Toyoda N, Kirkpatrick A. 2001. Materials processing by gas cluster ion beams. *Mater. Sci. Eng. R Rep.* 34:231–95
51. Bich C, Havelund R, Moellers R, Touboul D, Kollmer F, et al. 2013. Argon cluster ion source evaluation on lipid standards and rat brain tissue samples. *Anal. Chem.* 85:7745–52
52. Fletcher JS, Rabbani S, Barber AM, Lockyer NP, Vickerman JC. 2013. Comparison of C_{60} and GCIB primary ion beams for the analysis of cancer cells and tumour sections. *Surf. Interface Anal.* 45:273–76
53. Shon HK, Yoon S, Moon JH, Lee TG. 2016. Improved mass resolution and mass accuracy in TOF-SIMS spectra and images using argon gas cluster ion beams. *Biointerphases* 11:02A321
54. Angerer TB, Blenkinsopp P, Fletcher JS. 2015. High energy gas cluster ions for organic and biological analysis by time-of-flight secondary ion mass spectrometry. *Int. J. Mass Spectrom.* 377:591–98
55. Sämfors S, Ståhlman M, Klevstig M, Borén J, Fletcher JS. 2017. Localised lipid accumulation detected in infarcted mouse heart tissue using ToF-SIMS. *Int. J. Mass Spectrom.* 437:77–86
56. Angerer TB, Magnusson Y, Landberg G, Fletcher JS. 2016. Lipid heterogeneity resulting from fatty acid processing in the human breast cancer microenvironment identified by GCIB-ToF-SIMS imaging. *Anal. Chem.* 88:11946–54
57. Hannestad JK, Höök F, Sjövall P. 2018. Nanometer-scale molecular organization in lipid membranes studied by time-of-flight secondary ion mass spectrometry. *Biointerphases* 13:03B408
58. Szakal C, Ugelow MS, Gorham JM, Konicek AR, Holbrook RD. 2014. Visualizing nanoparticle dissolution by imaging mass spectrometry. *Anal. Chem.* 86:3517–24
59. Parry S, Winograd N. 2005. High-resolution TOF-SIMS imaging of eukaryotic cells preserved in a trehalose matrix. *Anal. Chem.* 77:7950–57
60. Carado A, Passarelli MK, Kozole J, Wingate JE, Winograd N, Loboda AV. 2008. C_{60} secondary ion mass spectrometry with a hybrid-quadrupole orthogonal time-of-flight mass spectrometer. *Anal. Chem.* 80:7921–29
61. Morales-Soto N, Dunham SJB, Baig NF, Ellis JF, Madukoma CS, et al. 2018. Spatially dependent alkyl quinolone signaling responses to antibiotics in *Pseudomonas aeruginosa* swarms. *J. Biol. Chem.* 293:9544–52
62. Smith DF, Robinson EW, Tolmachev AV, Heeren RMA, Paša-Tolić L. 2011. C_{60} secondary ion Fourier transform ion cyclotron resonance mass spectrometry. *Anal. Chem.* 83:9552–56
63. Fletcher JS, Rabbani S, Henderson A, Blenkinsopp P, Thompson SP, et al. 2008. A new dynamic in mass spectral imaging of single biological cells. *Anal. Chem.* 80:9058–64
64. Fisher GL, Bruinen AL, Ogrinc Potočnik N, Hammond JS, Bryan SR, et al. 2016. A new method and mass spectrometer design for TOF-SIMS parallel imaging MS/MS. *Anal. Chem.* 88:6433–40
65. Passarelli MK, Pirkl A, Moellers R, Grinfeld D, Kollmer F, et al. 2016. The 3D OrbiSIMS-label-free metabolic imaging with subcellular lateral resolution and high mass-resolving power. *Nat. Methods* 14:1178–83
66. Fletcher JS, Kotze HL, Armitage EG, Lockyer NP, Vickerman JC. 2013. Evaluating the challenges associated with time-of-fight secondary ion mass spectrometry for metabolomics using pure and mixed metabolites. *Metabolomics* 9:535–44

67. Phan NTN, Munem M, Ewing AG, Fletcher JS. 2017. MS/MS analysis and imaging of lipids across *Drosophila* brain using secondary ion mass spectrometry. *Anal. Bioanal. Chem.* 409:3923–32
68. Shi Y, Johnson J, Wang B, Chen B, Fisher GL, et al. 2019. Mass spectrometric imaging reveals temporal and spatial dynamics of bioactive lipids in arteries undergoing restenosis. *J. Proteome Res.* 18:1669–78
69. Sämfors S, Ewing AG, Fletcher JS. 2018. Benefits of NaCl addition for ToF-SIMS analysis including the discrimination of diacylglyceride and triacylglyceride ions. *Rapid Commun. Mass Spectrom.* 32:1473–80
70. Lanekoff I, Kurczy ME, Hill R, Fletcher JS, Vickerman JC, et al. 2010. Time of flight mass spectrometry imaging of samples fractured in situ with a spring-loaded trap system. *Anal. Chem.* 82:6652–59
71. Hill R, Blenkinsopp P, Thompson S, Vickerman J, Fletcher JS. 2011. A new time-of-flight SIMS instrument for 3D imaging and analysis. *Surf. Interface Anal.* 43:506–9
72. Angerer TB, Pour MD, Malmberg P, Fletcher JS. 2015. Improved molecular imaging in rodent brain with time-of-flight-secondary ion mass spectrometry using gas cluster ion beams and reactive vapor exposure. *Anal. Chem.* 87:4305–13
73. Angerer TB, Mohammadi AS, Fletcher JS, 2016. Optimizing sample preparation for anatomical determination in the hippocampus of rodent brain by ToF-SIMS analysis. *Biointerphases* 11:02A319
74. Le MUT, Son JG, Shon HK, Park JH, Lee SB, Lee TG. 2018. Comparison between thaw-mounting and use of conductive tape for sample preparation in ToF-SIMS imaging of lipids in *Drosophila* microRNA-14 model. *Biointerphases* 13:03B414
75. Tian H, Sparvero LJ, Amoscato AA, Bloom A, Bayir H, et al. 2017. Gas cluster ion beam time-of-flight secondary ion mass spectrometry high-resolution imaging of cardiolipin speciation in the brain: identification of molecular losses after traumatic injury. *Anal. Chem.* 89:4611–19
76. Tian H, Sparvero LJ, Amoscato AA, Bloom A, Bayır H, et al. 2017. Gas cluster ion beam time-of-flight secondary ion mass spectrometry high-resolution imaging of cardiolipin speciation in the brain: identification of molecular losses after traumatic injury. *Anal. Chem.* 89:4611–19
77. Thompson CE, Ellis J, Fletcher JS, Goodacre R, Henderson A, et al. 2006. ToF-SIMS studies of *Bacillus* using multivariate analysis with possible identification and taxonomic applications. *Appl. Surf. Sci.* 252:6719–22
78. Fletcher JS, Henderson A, Jarvis RM, Lockyer NP, Vickerman JC, Goodacre R. 2006. Rapid discrimination of the causal agents of urinary tract infection using ToF-SIMS with chemometric cluster analysis. *Appl. Surf. Sci.* 252:6869–74
79. Vaidyanathan S, Fletcher JS, Goodacre R, Lockyer NP, Micklefield J, Vickerman JC. 2008. Subsurface biomolecular imaging of *Streptomyces coelicolor* using secondary ion mass spectrometry. *Anal. Chem.* 80:1942–51
80. Wehrli PM, Angerer TB, Farewell A, Fletcher JS, Gottfries J. 2016. Investigating the role of the stringent response in lipid modifications during the stationary phase in *E. coli* by direct analysis with time-of-flight-secondary ion mass spectrometry. *Anal. Chem.* 88:8680–88
81. Nilsson KD, Palm M, Hood J, Sheriff J, Farewell A, Fletcher JS. 2019. Chemical changes on, and through, the bacterial envelope in *Escherichia coli* mutants exhibiting impaired plasmid transfer identified using time-of-flight secondary ion mass spectrometry. *Anal. Chem.* 91:11355–61
82. Tian H, Sparvero LJ, Blenkinsopp P, Amoscato AA, Watkins SC, et al. 2019. Secondary-ion mass spectrometry images cardiolipins and phosphatidylethanolamines at the subcellular level. *Angew. Chem.* 131:3188–93
83. Sheraz née Rabbani S, Barber A, Fletcher JS, Lockyer NP, Vickerman JC. 2013. Enhancing secondary ion yields in time of flight-secondary ion mass spectrometry using water cluster primary beams. *Anal. Chem.* 85:5654–58
84. Sheraz S, Barber A, Berrueta Razo I, Fletcher JS, Lockyer NP, Vickerman JC. 2014. Prospect of increasing secondary ion yields in ToF-SIMS using water cluster primary ion beams. *Surf. Interface Anal.* 46:51–53
85. Razo IB, Sheraz S, Henderson A, Lockyer NP, Vickerman JC. 2015. Mass spectrometric imaging of brain tissue by time-of-flight secondary ion mass spectrometry—How do polyatomic primary beams C_{60}^+, Ar_{2000}^+, water-doped Ar_{2000}^+ and $(H_2O)_{6000}^+$ compare? *Rapid Commun. Mass Spectrom.* 29:1851–62

86. Mouhib T, Delcorte A, Poleunis C, Bertrand P. 2010. Organic secondary ion mass spectrometry: signal enhancement by water vapor injection. *J. Am. Soc. Mass Spectrom.* 21:2005–10
87. Conlan XA, Lockyer NP, Vickerman JC. 2006. Is proton cationization promoted by polyatomic primary ion bombardment during time-of-flight secondary ion mass spectrometry analysis of frozen aqueous solutions? *Rapid Commun. Mass Spectrom.* 20:1327–34
88. Piwowar AM, Fletcher JS, Kordys J, Lockyer NP, Winograd N, Vickerman JC. 2010. Effects of cryogenic sample analysis on molecular depth profiles with TOF-secondary ion mass spectrometry. *Anal. Chem.* 82:8291–99
89. Sheraz S, Tian H, Vickerman JC, Blenkinsopp P, Winograd N, Cumpson P. 2019. Enhanced ion yields using high energy water cluster beams for secondary ion mass spectrometry analysis and imaging. *Anal. Chem.* 91:9058–68
90. Chandra S, Ausserer WA, Morrison H. 1987. Evaluation of matrix effects in ion microscopic analysis of freeze-fractured, freeze-dried cultured cells. *J. Microsc.* 148:223–39
91. Chandra S, Morrison GH. 1995. Imaging ion and molecular transport at subcellular resolution by secondary ion mass spectrometry. *Int. J. Mass Spectrom. Ion Process.* 143:161–76
92. Chandra S, Morrison GH. 1997. Evaluation of fracture planes and cell morphology in complementary fractures of cultured cells in the frozen-hydrated state by field-emission secondary electron microscopy: feasibility for ion localization and fluorescence imaging studies. *J. Microsc.* 186:232–45
93. Chandra S, Smith DR, Morrison GH. 2000. Subcellular imaging by dynamic SIMS ion microscopy. *Anal. Chem.* 72:104A–14A
94. Levi-Setti R, Gavrilov KL, Neilly ME, Strick R, Strissel PL. 2006. High resolution SIMS imaging of cations in mammalian cell mitosis, and in *Drosophila* polytene chromosomes. *Appl. Surf. Sci.* 252:6907–16
95. Zhang DS, Piazza V, Perrin BJ, Rzadzinska AK, Poczatek JC, et al. 2012. Multi-isotope imaging mass spectrometry reveals slow protein turnover in hair-cell stereocilia. *Nature* 481:520–24
96. Wedlock LE, Kilburn MR, Liu R, Shaw JA, Berners-Price SJ, Farrell NP. 2013. NanoSIMS multielement imaging reveals internalisation and nucleolar targeting for a highly-charged polynuclear platinum compound. *Chem. Commun.* 49:6944–46
97. Angelo M, Bendall SC, Finck R, Hale MB, Hitzman C, et al. 2014. Multiplexed ion beam imaging of human breast tumors. *Nat. Med.* 20:436–42
98. Frisz JF, Klitzing HA, Lou K, Hutcheon ID, Weber PK, et al. 2013. Sphingolipid domains in the plasma membranes of fibroblasts are not enriched with cholesterol. *J. Biol. Chem.* 288:16855–61
99. Yeager AN, Weber PK, Kraft ML. 2016. Three-dimensional imaging of cholesterol and sphingolipids within a Madin-Darby canine kidney cell. *Biointerphases* 11:02A309
100. Lanekoff I, Sjövall P, Ewing AG. 2011. Relative quantification of phospholipid accumulation in the PC12 cell plasma membrane following phospholipid incubation using TOF-SIMS imaging. *Anal. Chem.* 83:5337–43
101. Philipsen MH, Sämfors S, Malmberg P, Ewing AG. 2018. Relative quantification of deuterated omega-3 and-6 fatty acids and their lipid turnover in PC12 cell membranes using TOF-SIMS. *J. Lipid Res.* 59:2098–107